3

Freeboard Aerodynamic Phenomena

This chapter presents the rotary kiln freeboard aerodynamic phenomena, drawing parallels with fluid flow in conduits. The goal is to describe the characteristics of confined jets that determine burner aerodynamic mixing and, in turn, combustion efficiency, and flame shape and its character. Having described the flow field, the effect of turbulence on dust pick-up from the bed's free surface will also be discussed.

Fluid flow through the kiln freeboard comes from several sources, including combustion air, combustion products, and the air infiltrated into the vessel. In direct-fired kilns, especially those with pulverized fuel (p.f.) combustion systems, the fuel, for example, pulverized coal, is introduced from a pipe. Burner pipe nozzles range from 25–61 cm (10–24 in.) diameter in size and the kilns (combustion chamber) into which the fuel is discharged are typically 2.4–6.2 m (8–20 ft) in diameter. Hence with a chamber much larger than the burner pipe, the fuel emerges as a jet. The freeboard flow phenomenon near the combustion zone therefore exhibits the properties of jets, how they are entrained, and how they mix with the surrounding fluid. Therefore, the gross pattern of flow in the region near the burner is determined by the geometry or the physical boundaries surrounding the burner, typically involving a jet confined in a cylindrical vessel and by the manner in which the fuel is discharged. In order to prevent pulverized fuel from settling in pipes the conveying air (primary combustion

air) is introduced at a high velocity, typically greater than 30 m/s. For direct-fired rotary kilns the primary air usually comprises about 25% of the combustion air requirements. The secondary air makes up for the remaining 75% of the combustion air. The latter may be introduced through the inlet surrounding the primary air or from discharge coolers that recuperate some of the energy in the discharge product and return it into the kiln to improve combustion and fuel efficiencies. In the region further away from the combustion zone, the flow field is made up of combustion products and any other gases that are released as a result of the bed reactions. The combustion products must be induced into air pollution control devices to be cleaned up before discharge into the atmosphere. Atmospheric discharge is accomplished by an induced draft (I.D.) fan, which, as its name implies, induces gas flow through the kiln and controls the overall pressure drop across it. Because the I.D. fan pulls gas through the kiln, the kiln system is under suction and establishes a negative pressure drop across it. The fan's electrical current draw is usually a good indicator of the pressure drop and for that matter the gas flow rate. The higher the pressure (i.e., more negative) the greater the fan amperage. Owing to a slight vacuum, air infiltration into the kiln is almost always evident, originating from the joints between the cylinder and around the fire hood. Infiltration air also comes from several sources including kiln attachments, intended or unintended open access points, such as cleavages around burners, take-off pipes, holes, and so on, with the quantity dependent upon the efficiency of the seals around these curvatures. Kiln seals are therefore a big design and operational challenge, the most prominent being the point between the stationary fire hood and the rotating cylinder. It can be rightfully said that the kiln is like a big conduit and the I.D. fan drives the flow through it. The flow area (kiln freeboard) depends on the kiln loading or the degree of fill, thereby determining the turbulent intensity of the freeboard flow in the region further away from the combustion zone. Near the feed end the high turbulent kinetic energy can result in increases in dust generation and discharge through the exhaust. In the near field, however, the interaction of the primary air jet and secondary air in a confined environment introduces intense mixing involving recirculation eddies that return combustion products into the flame region, a phenomenon that underlies mixing, the mainstay of turbulent diffusion flames found in rotary kilns. Such flow properties exhibited by confined jets underlie the freeboard aerodynamic phenomena and will be described further in more detail.

3.1 Fluid Flow in Pipes: General Background

Gas flow downstream from the entry region in kilns follows fundamental principles similar to the generalized pipe flow laws. However, it is more complex in the near field involving entrained jets. These principles are based on the ideal gas laws that demand that $PV/T = constant$ for a nonreacting gas. Therefore, changes in any of the variables P, V, or T will result in a change in the others and will affect the demand on the I.D. fan. Most theoretical considerations in fluid dynamics are based on the concept of perfect fluids thereby requiring that the fluid is frictionless and incompressible. The no-slip condition in an incompressible fluid means that two contacting layers acting on each other exert only normal or pressure forces but not tangential forces or shear stresses. However, this assumption falls short in real fluids since they offer internal resistance to a change in shape. This results in the concept of viscosity whereby the existence of intermolecular interactions causes the fluid to adhere to the solid walls containing them. Because shear stresses are small for fluids of practical importance such as that encountered in rotary kilns their coefficients of viscosity are small and agree with perfect fluids. For more on the outline of fluid motion with friction the reader is referred to Schlichting (1979).

The nature of viscosity can be best illustrated by the velocity distribution between two plates, that is, Couette flow (Figure 3.1). The fluid motion is supported by applying a tangential force to the upper plate. Here, the fluid velocity is proportional to the distance, y, between the plates such that

$$u(y) = \frac{y}{h}U \tag{3.1}$$

The frictional force per unit area or the frictional shear stress, τ, is directly proportional to velocity, U, and inversely proportional to the spacing h yielding

$$\tau = \mu\frac{\mathrm{d}u}{\mathrm{d}y}, \tag{3.2}$$

where the constant of proportionality μ is the dynamic viscosity in units of kg/m · s, a property of the fluid. In all fluid motion where frictional and inertia forces interact, such as gas flows in rotary kilns,

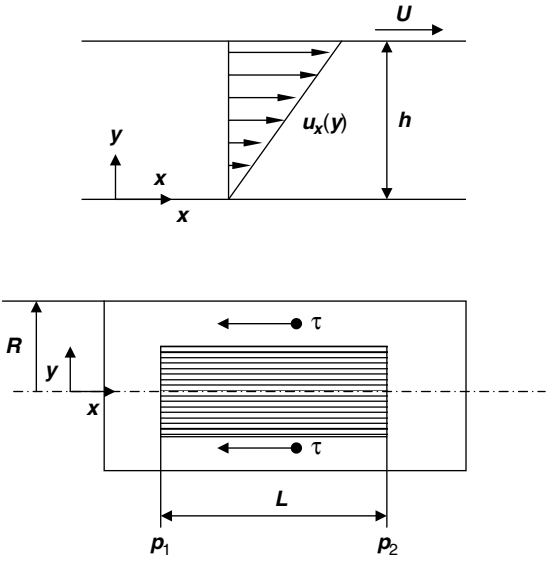

Figure 3.1 Couette flow.

kinematic viscosity, ν, is defined as the ratio between the dynamic viscosity and fluid density.

$$\nu = \frac{\mu}{\rho} \tag{3.3}$$

These frictional laws that define the viscosity can be applied to flow conditions in cylindrical pipes, in part, similar to conditions in rotary kilns. Fluid flow in conduits were first described by Reynolds' early experiments that identified the flow regimes as *laminar* and *turbulent*. For pipes, rotary kilns included, these are characterized by the relationships between pressure drop and flow rate. Laminar flows are characterized by the first Reynolds' principle, which states that the pressure drop of a flowing fluid is proportional to the flow rate at low velocities. We explore this principle in kilns in several ways. For example, a common practice of the industry is the use of a pitot tube for flow measurements during kiln audits. At high velocities, however, the pressure drop of a flowing fluid is proportional to roughly the square of the flow rate, that is, for turbulent flows. The transition regime between laminar and turbulent flows is defined by the Reynolds number, $Re = uD/\mu$. In laminar flow the fluid moves under the influence of an axial pressure gradient and the individual fluid layers act on each other with shear stress proportional to the velocity gradient. Because

there is no pressure gradient in the lateral direction the flow is streamlined, which by definition means that for each streamline the velocity is constant. The flow is accelerated by pressure and retarded by shear stress as shown in the classical Couette flow situation (Figure 3.1). Under these conditions the equilibrium condition in the flow direction, x, requires that the pressure forces acting on the cylinder cross section, that is, $(p_1 - p_2)\pi y^2$ must be balanced by the shear stress acting on circumference $2\pi yl \cdot \tau$ resulting in

$$\tau = \frac{p_1 - p_2}{l} \cdot \frac{y}{2} \tag{3.4}$$

Invoking the friction laws, Equation (3.2), and noting that the u decreases with y results in

$$\frac{\mathrm{d}u}{\mathrm{d}y} = -\frac{p_1 - p_2}{\mu l} \cdot \frac{y}{2} \tag{3.5}$$

This, upon integration, leads to the velocity distribution

$$u(y) = \frac{p_1 - p_2}{\mu l}\left(C - \frac{y^2}{4}\right) \tag{3.6}$$

The integration constant can be obtained by invoking the no slip condition at the wall, that is, $u = 0$ at $y = R$ for $C = R^2/4$ therefore resulting in a parabolic velocity distribution over the radius as

$$u(y) = \frac{p_1 - p_2}{4\mu l}\left(R^2 - y^2\right) \tag{3.7}$$

The maximum velocity is at $y = 0$, the centerline, i.e.,

$$u_{\mathrm{m}} = \frac{p_1 - p_2}{4\mu l}R^2 \tag{3.8}$$

The volume flow rate can be evaluated recognizing that the volume of the paraboloid of revolution is 1/2 times the base times the height which leads to the Hagen-Poiseuille equation of laminar flow through pipes (Schlichting, 1979) as follows:

$$Q = \frac{\pi}{2}R^2 u_{\mathrm{m}} = \frac{\pi R^4}{8\mu l}(p_1 - p_2) \tag{3.9}$$

Equation (3.9) restates the first Reynolds' experimental characterization indicating that for laminar flows in conduits and pipes, the flow rate is proportional to the first power of the pressure drop per unit length.

Equation (3.9) also states that the flow rate is proportional to the fourth power of the radius of the pipe.

For two flows of different fluids, different velocities, and different linear dimensions to be dynamically similar, it is necessary that the forces acting on the fluid particles at all geometrically similar points have a constant ratio at any given time. If we assume a simplified fluid flow, such as incompressible flow that has no elastic and gravitational forces, then the similarity of flows may satisfy the Reynolds' criterion that the ratio of the inertia and frictional forces is the same. The Reynolds' analogy can be derived by resolving the forces on a control volume in a steady parallel flow in the x-direction, where the magnitude of the inertia forces per unit volume is $\rho u \partial u/\partial x$. The resultant shear force in a control volume $(dx \cdot dy \cdot dz)$ is $\partial\tau/\partial y(dx \cdot dy \cdot dz)$, which is, on a per unit volume basis, equal to $\partial\tau/\partial y$. Invoking Equation (3.2) into it gives $\mu\partial^2 u/\partial y^2$. Consequently, for a condition of similarity, the ratio of the inertia forces to the frictional (viscous) forces, identified as the Reynolds number, must be the same.

$$\text{Inertia Forces/Friction Force} = \frac{\rho u \partial u/\partial x}{\mu \partial^2 u/\partial y^2} = \frac{\rho U^2/d}{\mu U/d^2} \tag{3.10}$$

$$Re = \frac{\rho U d}{\mu} = \frac{U d}{\nu} \tag{3.11}$$

thereby establishing the Reynolds' principle of similarity as was earlier derived.

Most practical flows are turbulent. The type of flow for which Equation (3.9) applies exists in reality only for small radius cylinders and for very slow flows with $Re < 2300$. The Reynolds number of the flow in large cylinders and vessels encountered in practical engineering applications such as rotary kilns are higher. With pipe diameters in the 2–5 m range, the Reynolds number after uniform velocity is attained in rotary kilns is typically on the order of 1.5×10^5 (Field et al., 1967) which falls well into the turbulent regime. For turbulent flows, the pressure drop is no longer directly proportional to the mean velocity but approximately proportional to the second power of the velocity. During transition from laminar into the turbulent regime, the velocity distribution becomes unstable in the presence of small disturbances. After the transition the laminar or the streamline structure disappears and the velocity at any point in the stream varies with time in both magnitude and direction as turbulent eddies form and decay. At this

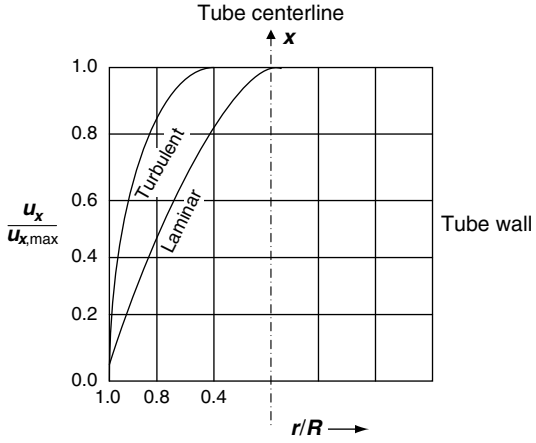

Figure 3.2 Qualitative comparison of laminar and turbulent velocity distribution.

point the ability of the fluid to transport momentum, energy, and mass in the mean flow direction is greatly enhanced (Figure 3.2). However, a considerable pressure difference is required to move the fluid through the kiln. This is in part due to the fact that the phenomenon of turbulent mixing dissipates large quantities of energy, which, in turn, causes an increase in the resistance to flow.

Theoretical relationships between fluid flow rate and pressure drop for turbulent flow in pipes of interest similar to that established for laminar flows are not readily available. However, empirical relations based on experiments have been fitted long ago by pioneers such as Blasius and others to provide quantitative assessment of frictional resistances in terms of *Re* (Schlichting, 1979). The velocity profile for turbulent flow in large pipes can be characterized as

$$\frac{u}{U} = \left(\frac{y}{R}\right)^{\frac{1}{n}} \tag{3.12}$$

where n is derived from experiment. The correlation between the shear stress at the wall and the flow velocity has been described as

$$\tau_0 = 0.03325\rho\bar{u}^{7/4}\nu^{1/4}R^{-1/4} = \rho u_*^2 \tag{3.13}$$

where

$$\frac{u}{u_*} = 8.74\left(\frac{yu_*}{\nu}\right)^{\frac{1}{7}} \tag{3.14}$$

and $\frac{yu_*}{\nu} > 70$ is a condition for purely turbulent friction. The expression for friction velocity can be derived as

$$u_* = 0.150u^{\frac{7}{8}}\left(\frac{\nu}{y}\right)^{1/8} \tag{3.15}$$

From which the local skin friction coefficient can be expressed as

$$C'_{\mathrm{f}} = \frac{\tau_0}{\frac{1}{2}\rho U^2} = 0.045\left(\frac{UR}{\nu}\right)^{-1/4} \tag{3.16}$$

Although these relations have no direct application to determining flow in the turbulent regime of the rotary kiln, they can be of help in estimating dust loss and wall heat transfer coefficients.

3.2 Basic Equations of Multicomponent Reacting Flows

Consistent with the objective of this chapter, it is important to return to the type of flow encountered in the freeboard of the rotary kiln and address reacting flows. The freeboard flow of interest involves the reacting flow type, which is almost always multicomponent, composed of fuel, oxidizer, combustion products, particulates, and so forth. The thermodynamic and transport properties of multicomponent reacting fluids are functions, not only of temperature and pressure, but also of species concentration. The basic equations that describe the simplest case of reacting turbulent flow include conservation equations for mass, concentration, momentum, and enthalpy equations as well as the associated reaction and equations of state for the system (Zhou, 1993),

$$\text{Continuity Equation: } \frac{\partial \rho}{\partial t} + \frac{\partial}{\partial x_j}\left(\rho u_j\right) = 0 \tag{3.17}$$

$$\text{Momentum Equation: } \frac{\partial}{\partial t}\left(\rho u_i\right) + \frac{\partial}{\partial x_j}\left(\rho u_j u_i\right) = -\frac{\partial P}{\partial x_i} + \frac{\partial}{\partial x_j}\left[\mu\left(\frac{\partial u_j}{\partial x_i} + \frac{\partial u_i}{\partial x_j}\right)\right] + \rho g_i \tag{3.18}$$

$$\text{Concentration Transport Equation: } \frac{\partial}{\partial t}(\rho Y_s) + \frac{\partial}{\partial x_j}(\rho u_j Y_s) = \frac{\partial}{\partial x_j}\left(D\rho \frac{\partial Y_s}{\partial x_j}\right) - w_s \tag{3.19}$$

$$\text{Enthalpy Transport Equation: } \frac{\partial}{\partial t}(\rho c_p T) + \frac{\partial}{\partial x_j}(\rho u_j c_p T) = \frac{\partial}{\partial x_j}\left(\lambda \frac{\partial T}{\partial x_j}\right) + w_s Q_s \tag{3.20}$$

$$\text{Arrhenius Equation: } w_s = B\rho^2 Y_F Y_{ox} \exp(-E/RT) \tag{3.21}$$

$$\text{Equation of State: } P = \rho RT \sum Y_s/M_s \tag{3.22}$$

We will examine how some commercially available computational tools are used to solve such a system of equations but for the kiln engineer, perhaps the physical interpretation underlying these complex equations are most important. The similarity parameters inferred from these equations might allow the engineer to make some judgments of what aspects of the flow matter in burner design and operation. Using the momentum and the energy equations, similarity parameters for reacting flows can be obtained as follows:

1. For fluid flow, the Euler number might be defined as the ratio of the pressure head and the velocity head and is expressed as:

$$Eu = \frac{P_\infty}{\rho_\infty U_\infty{}^2} \tag{3.23}$$

2. As we saw earlier, the Reynolds number represents the ratio of the inertial force and the viscous force, that is,

$$Re = \frac{U_\infty L}{\nu_\infty} \tag{3.24}$$

3. The Mach number is a similarity parameter defined as the ratio between kinetic energy and thermal energy.

$$Ma = \sqrt{\frac{U_\infty{}^2/2}{c_p T_\infty}} \approx \frac{U_\infty}{a} \tag{3.25}$$

4. For heat transfer within the fluid the similarity parameter of importance is the Peclet number, which is the ratio of heat convection and heat conduction. We will revisit heat transfer modes later but for the purposes of flow characterization, the Peclet number is defined in Equation (3.26) below, where it is also given as the product of the Reynolds number and the Prandtl number, *Pr* (kinematic viscosity ≠ thermal diffusivity)

$$Pe = \frac{\rho_\infty U_\infty c_p / L}{\lambda_\infty T_\infty / L} = \frac{U_\infty L}{\lambda_\infty / \left(c_p \rho_\infty\right)} = Re \cdot Pr \tag{3.26}$$

5. There are two dimensionless parameters for freeboard combustion and they are the Damkohler I and II, which compare, respectively, the time it will take the reacting fluid to travel the combustion chamber to the reaction time; and the time it takes the reacting molecules to diffuse to the reaction front and the reaction time.

   a. Damkohler I – (heat of reaction)/(heat of convection) = (flow time)/(reaction time)

$$D_I = \frac{w_{s\infty} Q_s}{\rho_\infty U_\infty c_p / L} = \frac{\tau_f}{\tau_c} \tag{3.27}$$

   b. Damkohler II – (heat of reaction)/(heat of conduction) = (diffusion time)/(reaction time)

$$D_{II} = \frac{w_{s\infty} Q_s}{\lambda_\infty T_\infty / L^2} = \frac{\tau_d}{\tau_c} \tag{3.28}$$

We will treat freeboard combustion later on but suffice it to say that the flow patterns encountered in the combustion zone of a rotary kiln play the most important role in efficient combustion, particularly with pulverized fuel combustion. As the Damkohler numbers indicate, the time scale of combustion involves the diffusion time and the chemical reaction times. Since the reaction will occur when the reactants (air and fuel) are brought together, diffusion is the rate controlling time step in the combustion process. In turbulent diffusion flames, the controlling measure is the mixing time scale induced by the recirculation eddies of the primary air jet. The conventional wisdom in combusting fluid is that "if it is mixed, it is burnt." As a result, much of the combustion characteristics can be inferred and characterized by the mixing strengths without even resorting to the solution of the full systems of equations presented here in Equations (3.17–3.22). We will

begin with the characterization of the properties of jets as introduced from a primary air pipe into the larger kiln surroundings and discuss the mixing of the flow in the confined region of the kiln as it induces the secondary air from within.

3.3 Development of a Turbulent Jet

It was mentioned earlier that the sources of fluid flow in rotary kilns are the primary air, secondary air, combustion products, and infiltration air. Usually the combustion system is such that the primary air issues from a burner nozzle as a jet into an open tube or into a tube surrounded with secondary air prior to combustion. The primary air nozzle tip velocities can be anywhere between 20 m/s and 100 m/s depending on the firing rate. The secondary air into which the primary air is discharged is at a relatively lower velocity, typically in the range of 5–15 m/s (Table 3.1).

The aerodynamic structure of the jet is therefore similar to a submerged free jet (Figure 3.3) except that the structure is distorted due to the boundary constraints of the kiln tube. Unlike a free jet, which has an infinite source of air to entrain, the confined jet (Figure 3.4) has a limited source of entrained fluid. Therefore, when the jet fluid (primary air) emerges from the nozzle, a surface discontinuity is formed between it and the surrounding fluid (secondary air). This discontinuity results in an unstable surface with waves developing on it that enlarge as they move downstream. They eventually grow into eddies that extend inward to the boundaries of the kiln roughly halfway

Table 3.1 Typical Values of Primary and Secondary Air Velocities and Temperatures

	Cement Kiln	Lime Kiln	Aggregate Kiln
Primary air			
Percent of total flow	25–30		15–20
Temperature, K	375		
Velocity, m/s	60–100	20–45	20–30
Secondary air			
Percent of total flow	70–75		
Temperature, K	750		
Velocity, m/s	5–15	5–10	5–10

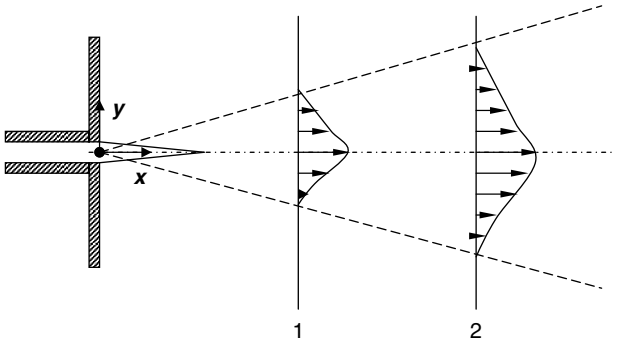

Figure 3.3 Turbulent free jet.

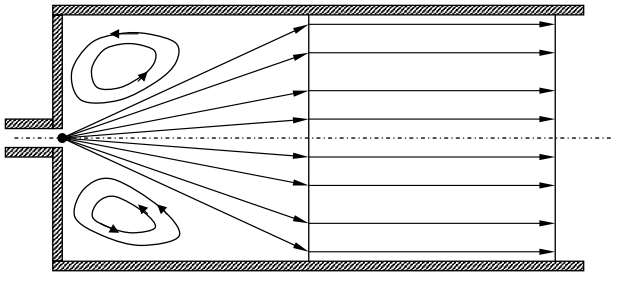

Figure 3.4 Turbulent confined jet.

between the horizontal axis and the outermost points. The boundary becomes distorted such that at any point within the volume occupied by eddies, there will be encountered at some time unmixed fluid from outside the jet, and at other times, fluid that is a mixture of jet fluid and the entrained surrounding fluid. For submerged jets, the unmixed surrounding fluid can be non-turbulent while the jet fluid is turbulent. The turbulence in the mixing region of the jet results from velocity gradients that are introduced by the large-scale eddies in the shear flow. If one considers a time-mean velocity component in the direction parallel to the axis of the jet, one will find in the turbulent free jet a characteristic sequence of development within the tip of the nozzle. By about eight nozzle diameters downstream the mean velocity profile is fully developed (Field et al., 1967). The stages of development include the potential core, which progressively diminishes in cross sectional area up to a second region, the transition region, which extends about 4–5 nozzle diameters before the fully turbulent region (Figure 3.3).

The theory of jets is not the subject of this work. The flow field can be fairly accurately predicted using computational fluid dynamic (CFD) software to mathematically model the conservation equations presented for reacting flows. However, successful analytical predictions of the behavior of jets have been made elsewhere by using certain assumptions concerning mass and momentum transfer, for example, Prandtl's mixing length theory. Such theories can provide useful expressions for the boundary layer velocity profile of free jets that can be applied without the rigor of CFD. However it might be said that the general characteristics of jets that have applications in rotary kiln combustors are turbulent diffusion jets for which analytical solutions can be challenging and might require added experience. They can be distinguished from laminar jets by the random fluctuations of the velocity that are superimposed on the mean velocity field and also by the fact that energy dissipation occurs through eddies of various sizes including up to and below the 0.1 cm level and in which dissipation is predominantly by the process of molecular diffusion. Some of the velocity and concentration measurements carried out by early investigators such as van der Hegge Zijnen (1958), Ricou and Spalding (1961), and so on are still applicable today for establishing velocity profiles for free jets. For example the transverse velocity and concentration profiles can be established by the relationship for plain and round jet respectively as:

$$\frac{\bar{u}}{\bar{u}_m} = 0.5\left(1 + \cos\left\{\frac{\pi y}{2x\tan\varphi}\right\}\right) \tag{3.29}$$

$$\frac{\bar{u}}{\bar{u}_m} = 0.5\left(1 + \cos\left\{\frac{\pi r}{2x\tan\varphi}\right\}\right) \tag{3.30}$$

where φ is the jet half-angle, typically 5.5° for free plane (Equation 3.29) and round (Equation 3.30) jets. In any plane perpendicular to a round, free jet axis a relative measure of the entrained ambient fluid was established by Ricou and Spalding (1961) as the ratio of mass flow at x, m_x, to the mass at source, m_0, that is,

$$\frac{\dot{m}_x}{\dot{m}_0} = 0.508\left(\frac{\rho_a}{\rho_0}\right)^{1/2}\left(\frac{x}{h}\right)^{1/2} \tag{3.31}$$

For round jets, particularly pertinent to primary air discharge in rotary kilns, Ricou and Spalding derived the following equation,

$$\frac{\dot{m}_x}{\dot{m}_0} = 0.32 \left(\frac{\rho_a}{\rho_0}\right)^{1/2} \frac{x}{d_0} \tag{3.32}$$

Equation 3.32 is applicable to all values of Reynolds numbers at the nozzle greater than 2.5×10^4, and holds only for $x/d_0 \geq 6$. At shorter distances from the nozzle Ricou and Spalding expect that entrainment $(\dot{m}_x/\dot{m}_0 - 1)$ proceeds at a lower rate of travel along the jet axis and increases progressively until it stabilizes at a constant value.

3.4 Confined Jets

Perhaps the most applicable aerodynamic phenomenon to the rotary kiln combustion system is the confined jet. Unlike the free jet with its unlimited supply of entrainable fluid, when a jet is confined in an enclosed environment the free supply of surrounding fluid available for entrainment is cut off. The pressure within the jet increases with distance from the nozzle instead of remaining constant as it does in free jets, and the gas entrained in the region near the nozzle originates from the edge of the jet further downstream before the points where the jet impinges on the enclosing wall. The flow of gas back toward the nozzle and close to the surrounding walls is known as recirculation (Figure 3.4).

Recirculation plays a very important role in the shaping of turbulent diffusion flames encountered in rotary kilns. By the entrainment action of the confined jet the reactants are mixed with further secondary air and with recirculated combustion products. Within the jet the entrained fluid is mixed with the jet fluid by turbulent diffusion as described earlier. For example, in pulverized fuel combustion, the return of the combustion products by entrainment to the nozzle increases mixing and also the particle residence time in the reaction zone, thereby improving the heterogeneous gas–solid combustion reactions. Granted that such processes are characterized by the Damkohler numbers, Equations (3.27) and (3.28), the increased diffusional mixing will result in more complete combustion. Several studies including recent works at the International Flame Research Foundation (IFRF) in Ijmuiden, the Netherlands (Haas et al., 1998), have established a direct correlation between flame shape, intensity, and

heat flux with the extent of recirculation eddies in direct-fired pulverized fuel rotary kiln combustors. Because of its importance in tube combustion including rotary cement kilns, and the lack of computational fluid dynamic capabilities at the time, early flame researchers proposed simple theoretical treatment of the confined jet problem based on analytical and empirical relations of free jet entrainment. Some of these early works at IFRF dating as far back as 1953 have been well documented and are still in use today. The confined flame theory established by Thring and Newby (1953), Craya and Curtet (1955), and those that appeared later from the work of Becker (1961) have been used in establishing the optimum aerodynamic characteristics of confined flames. In the rotary cement kiln where the secondary air is introduced at lower velocities compared with the primary air, one can assume that the secondary air is introduced as a stream with negligible momentum and that it is wholly entrained by the primary air jet before any recirculating gas is entrained. Based on this assumption, Craya and Curtet developed a relation between the momentum ratios known as Craya-Curtet parameter using the similarity laws between free and confined jets. The parameter has found useful application in rotary kilns where it is used as a qualitative measure of the extent of recirculation of entrained gases. It serves as a surrogate to characterizing rotary kiln flame shapes and intensity without the rigor and the complexity of using CFD. The Craya-Curtet parameter is defined as (Jenkins and Moles, 1981):

$$M = \frac{3}{2}R^2 + R + \frac{KR^2}{(r_0/L)^2} \tag{3.33}$$

where R is the discharge ratio, q/Q; $q = (u_0 - u_a)r_0^2$; $Q = u_a(L - \delta^*)^2 + q$; K is a factor relating to the shape of the velocity profile; u_0 is the jet velocity and u_a is the surrounding fluid velocity, δ^* is the boundary layer displacement thickness defined as $1.74/\sqrt{Re}$; L is the half width of the combustion chamber (rotary kiln) duct; and r_0 is the radius of the jet nozzle.

While this parameter varies between unity and infinity, experience has shown that for short and intense flames encountered in cement kilns, the recirculation is such that the Craya-Curtet parameter $M \geq 2.0$. Flames with M between 1 and 2 are characterized as long flames with the intensity suitable for processes such as rotary limestone calcination kilns. For flames with $M \leq 1.0$, the entrainment is such that the flame tends to be long and lazy. The Craya-Curtet parameter,

Equation (3.33), is essentially the ratio between the primary air jet momentum and the secondary air momentum and is a measure of the aerodynamic mixing of the two streams. High primary air velocities will return more combustion products to the burner nozzle and will result in attached flames associated with high Craya-Curtet parameters. The parameter can also be changed by altering the secondary air conditions. We will return to the use of the Craya-Curtet parameter for qualitative assessment of mixing, flame shapes, and flame intensity later on in the discussion of freeboard combustion.

3.5 Swirling Jets

The use of swirling jets has long been one of the practical ways of inducing mixing and improving burner effectiveness in rotary kilns. The increased flame stability and intensity associated with swirls are due to improved recirculation vortex (vortex shedding) which, like high velocity primary air jets, returns hotter combustion gases to the flame front where they become entrained in the primary air fluid prior to ignition and this enables the transfer of energy to the incoming reactants. Swirl burners typically seek to stabilize the flame by establishing a central recirculation zone (CRZ) and an external recirculation zone (ERZ), as depicted in Figure 3.5.

Pulverized fuel combustion swirl jets improve particle residence time in the combustion zone, and consequently improve combustion efficiency. Increasing the swirl number and thereby the jet angle moves

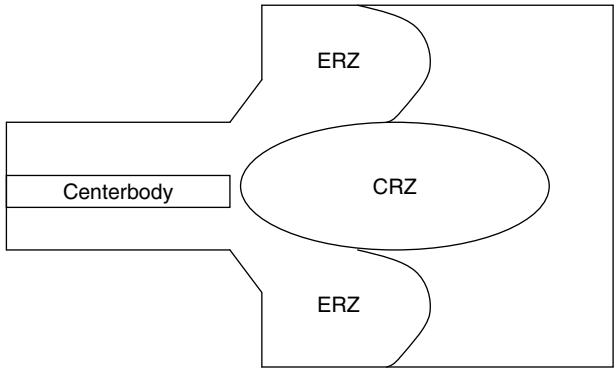

Figure 3.5 Schematic diagram of the effect of swirl on jet aerodynamics. CRZ, central recirculation zone; ERZ, external recirculation zone.

the external recirculation eddy (vortex shedding) closer to the burner in most kiln flames and results in flame attachment. Essentially, swirl can provide conditions that can approach a well-stirred reaction zone in combustion systems. The centrifugal effect of the swirling jet induces a reduced pressure along the axis close to the burner and an increased pressure further downstream resulting in an axial recirculation eddy. The intensity of the swirling jet is characterized by the swirl number, defined as the ratio of the angular momentum to the linear momentum flux

$$S = \dot{L}_0 / \left(\dot{G}_0 d_0 \right) \tag{3.34}$$

The nozzle flux of angular momentum, $\dot{L}_0$ and the flux of linear momentum $\dot{G}_0$ might be calculated as

$$\dot{L}_0 = 2\pi\rho \int_0^{r_0} \left(\vec{u}\vec{w} \right)_{\text{nozzle}} r^2 \mathrm{d}r \tag{3.35}$$

$$\dot{G}_0 = 2\pi \int_0^{r_0} \left(P + \rho \vec{u}^2 \right)_{\text{nozzle}} r \mathrm{d}r \tag{3.36}$$

where d_0 and r_0 are the respective nozzle diameter and radius, and P is the static or gauge pressure. P is included to allow for pressure variations due to centrifugal forces. Often times geometrical swirl number is defined in experimental setup as

$$S_g = \frac{r_0 \pi r_e}{A_t} \frac{Q_\tau^2}{Q_T^2} \tag{3.37}$$

where r_e is the radius at which the tangential inlets of the swirl vanes are attached with respect to the center axis and A_t is the total area of the tangential inlets. Q_τ and Q_T are the tangential flow rate and total flow rate respectively. It is found that S is directly proportional to S_g (Chatterjee, 2004). By altering the flow field and hence the strength of the recirculating zones, the flame can be induced to reside predominantly in either the recirculation zones or the shear layer between the zones.

3.6 Precessing Jets

Instead of using swirl generators, another method of generating vortex shedding, which has been found to increase radiant heat transfer, is by precessing the jet stream. A precessing jet flow can be generated either by an axisymmetric nozzle which utilizes a natural fluid

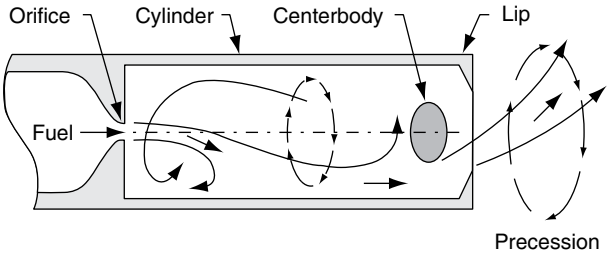

Figure 3.6 Precessing jet nozzle.

flow instability (Figure 3.6) or by a motor-driven mechanical nozzle (Nathan et al., 1996). The precessing jet nozzle provides a new method of mixing fuel and air together in a way similar to variable turbulent swirl generators. It has been established that this method of mixing has significant beneficial effects on combustion and on processes requiring combustion by significantly reducing pollution and simultaneously increasing radiant heat transfer. The invention is described in a patent (Luxton, Nathan, and Luminis, 1988) held by Adelaide Research and Innovation Pty. Ltd., of the University of Adelaide, and marketed to the rotary kiln industry as Gyro-Therm™. In its simplest form the nozzle is a cylinder with a small concentric inlet orifice at one end, and an axisymmetric lip at the other end. When the dimensions of the pressing jet nozzle fall within certain criteria defined by the Strouhal number, the jet flow through the inlet orifice is subjected to an unstable lateral deflection and attaches asymmetrically to the internal wall of the cylinder.

The exit lip at the nozzle exit then deflects the emerging eccentric jet so that it wobbles or precesses at a large angle to the nozzle axis (Nathan, Hill, and Luxton, 1998). The dimensionless Strouhal number of precession is defined as

$$St_p = f_p d_e / u_e \tag{3.38}$$

where f is the frequency of precession, d_e is the exit diameter, and u_e is the mean exit velocity. In the lower Strouhal number flow regime, $St_p < 0.01$, the cold-flow mixing characteristics are somewhat analogous to that of a fully pulsed jet. Here the time scale of the precession is large in comparison with the time scales associated with the movement of the entrained ambient fluid, so that there are no significant asymmetries in the pressure field surrounding the local jet. Under these conditions the dominant effect of the precessing motion of the jet is the superimposition of additional shear stress on the stresses that

already exists in the stationary jet. It has been established (Nathan et al., 1996) that the additional shear relates to the product of the rotation rate and sine of the jet deflection angle. Cold flow velocity measurements within 10 nozzle diameters of a precessing jet operating in the low-St_p (St_p = 0.002) regime have shown that the radial spread of the instantaneous jet, which is based on the jet half-width and phase-averaged at the precession frequency, is about three times that of a non-precessing jet. Schneider (1996) showed that at the low-St_p regime a precessing jet flame has been observed to be shorter and less luminous than either conventional jet flames or those at higher St_p. By contrast, for high Strouhal number flow ($St_p \geq 0.01$) the time scales associated with the precessing motion of the jet is comparable to time scales associated with the motion of entrained fluid within the region of space through which the jet precesses. Under these conditions, a low pressure zone is generated in the region between the jet and the nozzle axis, which also precesses with the jet. In such cases large streamline curvature can be observed in the phase-averaged flow field, along with a rate of decay in the mean velocity field which is an order of magnitude higher than that of a non-precessing jet flow (Schneider, 1996). Here, the largest scale of the turbulent flow is that of the path described by the motion of the precession, so that the phase-averaged radial spread of the instantaneous jet is now some seven times that of a non-precessing jet. Nathan et al. (1993) and Nathan and Luxton (1993) found an influence of the modified mixing characteristics on both the radiation heat flux and on NOx emissions for both open and confined flames. They claim to have demonstrated a reduction in NOx emissions on the order of 50–70% and a simultaneous increase in flame luminosity, an attribute that is important in radiation heat transfer in rotary kilns. It is proposed that due to the large eddy created by the precessing action described herein, natural gas can undergo cracking prior to combustion to generate soot particles which, in turn, proceed to combustion in a manner similar to pulverized fuel. In so doing the soot-laden flame emits radiant energy, a component of the heat transfer mechanism that is enhanced by the rotary kiln curvature. For example, it has been claimed that the first installation of a PJ burner at the Ash Grove Cement Plant in Durkee, Oregon increased the rotary kiln product output by 11%, increased specific fuel efficiency by 6%, and reduced NOx emissions by 37% (Videgar, 1997). This prompted the promotion and positioning of the Gyro-Therm™ as a low-NOx burner, however, subsequent installations at other locations have received mixed results in NOx emissions.

3.7 The Particle-laden Jet

An air jet laden with particles such as that found in primary air issuing from a pulverized fuel pipe for combustion in cement and lime kilns may be synonymous with a jet of fluid with density greater than air provided the particles are small enough that one can consider the fluid to be homogenous. Under such conditions the effect of the solid burden may be accounted for by simply assuming an increase in the gas density and a reduction in the kinematic viscosity. A concomitant result will be an accelerated turbulence and an intensification of mixing and the entrainment phenomena associated with it. Equation 3.32 applies in such situations whereby m_0 might be increased by the factor ρ_0/ρ_a owing to the presence of suspended solid so that the effective change in air entrained per unit volume of jet fluid might increase by a factor of $(\rho_0/\rho_a)^2$. When the particles are not small enough to behave like a homogeneous fluid, a relative motion occurs between the particles and the surrounding air as a result of gravity or as a result of inertial forces resulting in the damping of the turbulence since the drag between the dust and the air will extract energy from the turbulent fluctuations. One important estimate is the distance at which a particle in a particle-laden jet will travel before coming to rest. This distance is defined as the range λ, a product of the initial velocity of the particle and the relaxation time τ_R

$$\lambda = U_0 \tau_R \tag{3.39}$$

The relaxation time is defined here as the time taken for the relative velocity between particle and gas to fall to 36.8% of its initial value. For a perfect spherical particle, the relaxation time is defined as

$$\tau_R = \frac{m}{6\mu\pi r_p} \tag{3.40}$$

where m and r_p are the mass and radius of the particle, respectively, and μ is the dynamic viscosity of the surrounding fluid. With these definitions, one can estimate that coal particles with diameter of 80 micron injected at 60 m/s will have a range of about 150 cm, some 150 nozzle diameters for a 1-cm nozzle pipe, and will have little effect on the jet (Field et al., 1961). However, if the particles were finer, for example, 40 micron size, then the range would only be 30 cm which would have a damping effect on the jet due to turbulent energy transfer. The relaxation time is a measure of the shortest timescale of turbulence to

which the particle could respond. As mentioned earlier, smaller eddies would have rapid velocity fluctuations and the particles would not have time to accelerate to the velocities within the eddies. However, if the eddies are large, then the particles can follow the streamlines without any appreciable slip and the suspension would tend to behave as a homogeneous fluid. It has been shown that increasing the fluid temperature shortens the relaxation time and thereby reduces the size of the eddy to which particles respond. When it falls within the same range as the timescale of the eddies, some damping of the turbulence can be expected, thereby reducing the eddy viscosity (Field et al., 1967). The concomitant result will be a decrease in the rate of entrainment and the rate of spread of the turbulent jet.

3.8 Dust Entrainment

We have examined the effect of kiln aerodynamics on fluid mixing and combustion. It is equally important to look at the aerodynamic effect on dust carryover from rotary kilns processing mineral materials. Although the principles behind particle motion are related to granular flow which will be covered in Chapter 4, the interaction of the flow of fluid in the freeboard and the active layer surface of the kiln bed is an aerodynamic phenomenon.

The principle behind dust pickup is known as *saltation* and was first established by Bagnold in his study of sand dunes in deserts (Bagnold, 1941). If the particles are heavy enough and the gas velocity very high, the gas flow over the bed surface will induce a motion known as saltation in which individual grains ejected from the surface follow distinctive trajectories under the influence of gas velocity, resistance, and gravity. Because of their large size, these particles fail to enter into suspension. Instead, once lifted from the surface, they rise a certain distance, travel with the freeboard gas velocity, and descend; either to rebound on striking the surface or embed themselves in the surface and eject other particles (Figure 3.7).

The two principal underlying phenomena for saltation are: (i) that the layer behaves, so far as the flow outside it is concerned, as an aerodynamic roughness whose height is proportional to the thickness of the layer, and (ii) that the concentration of particles within the layer is governed by the condition that the shear stress borne by the fluid decreases, as the surface is approached, to a value just sufficient to ensure that the surface grains are in a mobile state (Owen, 1964).

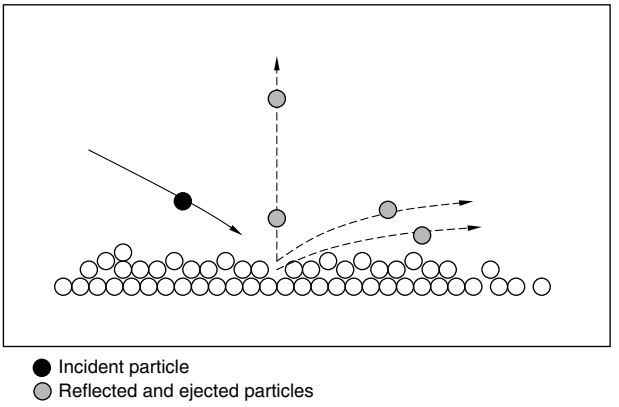

Figure 3.7 Concept of particle saltation (after Owen, 1964).

The first principle follows the analogy of the aerodynamic behavior of surface roughness and the velocity profile in the fluid outside the saltation layer follows the friction law

$$\frac{U}{u_\tau} = 2.5 \log\left(\frac{2gy}{u_\tau^2}\right) + D' \quad (y \geqslant h) \tag{3.41}$$

where U is the freeboard velocity at height y above the free surface, h is the thickness of the saltation layer, and D' is a constant. For wind over sand dunes, Owen (1964) fitted several experimental data presented earlier by Bagnold and others and established that $D' = 9.7$. The second principle postulates that the closer one gets to the surface the greater the amount of horizontal momentum transported vertically by the particles. Since the shear stress (the momentum transfer rate) must be constant throughout the saltation layer, the proportion carried by the fluid decreases. The skin friction τ_0 required to initiate movement among otherwise stationary grains is defined by the ratio β relating the hydrodynamic force on the surface to the weight of the particle

$$\beta = \frac{\tau_0}{\rho_p g d_p} \tag{3.42}$$

Bagnold (1941) determined two threshold values of β, a lower threshold value for which grain movement is first detected ($\beta = 0.01$), and an impact threshold at which saltation would be maintained ($\beta = 0.0064$). Hence the shear stress required near the surface to sustain an

equilibrium saltating flow is $\tau_0 = 0.0064\,\rho_p g d_p$. Finally, it may be stated that the saltation can be prescribed by the relationship

$$O\left(10^{-2}\right) < \frac{\rho_g u_\tau^2}{\rho_p g d_p} < O(1) \tag{3.43}$$

where the lower limit is required for surface mobility and the upper limit by the condition that grains do not enter into suspension.

The active layer surfaces encountered in rotary kilns are not stationary; rather, there is already a surface mobility due to the continuous surface renewal imposed by the particle cascades or excursions. The situation is even harder to model when kiln internals such as lifters and tumblers are installed. Nonetheless the aerodynamic condition expressed in Equation 3.43 is applicable by making modifications to the surface mobility through the density, perhaps, proportional to the granular dilation which we will discuss later in Chapter 4. Dust entrainment in rotary kilns requires several regimes of increasing freeboard velocity for a specified cut size distribution of particles. The velocity regimes include the two threshold saltation velocities, the minimum velocity required to pick up a saltating particle and transport it. Sood et al. (1972) used 2–2.5 times saltation velocity as the dust pickup velocity to estimate the entrainment for the design of a rotary coke calciner. They estimated the saltation velocity (in units of ft/s) using what they term a functional form of a dimensionless analysis relating the field parameters as

$$U_{\text{salt}} = 3.2 u_\tau \left(\frac{m_s}{m_g}\right)^{0.2} \left(\frac{D}{d_p}\right)^{0.6} \left(\frac{\rho_g}{\rho_p}\right)^{0.7} \left(\frac{u_s^2}{gD}\right)^{0.25} \tag{3.44}$$

where $u_s = m_s/A_s$ and the terminal velocity given by

$$u_\tau = \left[\frac{4}{3} g \frac{d_p\left(\rho_p - \rho_g\right)}{C_D \rho_g}\right]^{0.5} \tag{3.45}$$

where for the turbulent flow in the freeboard, $10^3 \le Re \le 10^5$, $C_D = 0.44$, that is, Newton's law regime. The dust pickup can be estimated by these correlations in the absence of CFD or without developing a true granular flow for the active layer as $U_{\text{dust}} = (2-2.5)U_{\text{salt}}$. That is, the dust entrainment velocity can be approximated by 2 to 2.5 times saltation velocity.

Other correlations for dust entrainment in rotary kilns have appeared in the literature (Li, 1974) but these are not easy to use for

estimating dust generation. Tackie et al. (1990) attempted to model dust entrainment in a rotary kiln by coupling a simplified form of the Navier-Stokes fluid dynamic equations in the freeboard and the saltating friction factor assuming a saltating layer of 2 cm. The predicted entrainment rate (defined, R_s) for a 3.5 m diameter kiln was presented. The model validation is not known and, to the author's knowledge, has not found any practical application in industrial rotary kilns.

3.9 Induced Draft Fan

The total flow through the kiln is induced by the large induced draft (I.D.) fan located at the outlet of the kiln system and prior to the stack. I.D. fans are called dirty fans because unlike forced draft fans for primary air, and other uses, I.D. fans handle the gases produced by combustion, dust that might be entrained and not collected in the bag filter, the excess air, and any infiltration air that occurs up to the fan inlet. As mentioned earlier, infiltration air comes from all sources including leaks directly into the rotary kiln and can be as high as 20% of the total gas mass flow through the kiln. This makes determining I.D. fan requirements more of an art than an exact science. Knowing the total mass flow, volume flow rate (e.g., ACFM) can be estimated and with some knowledge of the pressure drop (static pressure, given in units of in.-H_2O) across the system beginning from the hood to the fan inlet, the fan's performance or the required size can be estimated from readily available fan curves and/or calculations.

References

R. A. Bagnold. *Physics of Blown Sands and Desert Dunes*. William Morrow, New York, 1941.

H. A. Becker. *Concentration Fluctuation in Ducted Jet Mixing*. SC.D. Thesis, MIT, Cambridge, MA, 1961.

P. Chatterjee. *A Computational Fluid Dynamics Investigation of Thermoacoustic Instabilities in Premixed Laminar and Turbulent Combustion Systems*. Ph.D. Thesis, Virginia Polytechnic Institute and State University, Blacksburg, VA, 2004.

A. Craya and R. Curtet. "Sur L'evolution d'un Jet en Espace Confine," *Computes-Rendus de l'Academie des Sciences (C.R.A.S.)*, 241(1), 621–622, 1955.

M. A. Field, D. W. Gill, B. B. Morgan, and P. G. W. Hawksley. *Combustion of Pulverized Coal*. British Coal Utilization Research Association (BCURA), Leatherhead, UK, 1967.

J. Haas, A. Agostini, C. Martens, E. Carrea, and W. L. v. d. Kamp. *The combustion of Pulverized Coal and Alternative Fuels in Cement Kilns, Results on CEMFLAME-3 Experiments*. A Report, IFRF Doc. No. F97/y4, 1998.

B. G. Jenkins and F. D. Moles. "Modelling of Heat Transfer from a Large Enclosed Flame in a Rotary Kiln," *Trans. IChemE*, 59, 17–25, 1981.

K. W. Li. "Application of Khodrov's and Li's entrainment equations to rotary coke calciners," *AIChE J.*, 20(5), 1017–1020, 1974.

R. E. Luxton, G. J. Nathan, and Luminis Pty. Ltd. "Mixing of fluids," *Australian Patent Office*, Patent No. 16235/88, International Patent No. PCT/AU88/00114, 1988.

G. J. Nathan, S. Brumale, D. Protor, and R. E. Luxton. "NOx reduction in flames by modification of turbulence with jet precession." In *Combustion and Emissions Control* (N. Syred, Ed.) The Institute of Energy, pp. 213–230, 1993.

G. J. Nathan, S. J. Hill, and R. E. Luxton. "An axisymmetric fluidic nozzle to generate jet precession," *J. Fluid Mech.*, 370, 347–380, 1998.

G. J. Nathan and R. E. Luxton. "A low NOx burner with a radiant flame." In *Energy Efficiency in Process Technology* (P. A. Pilavacji, Ed., pp. 883–892), Elsevier, Inc., New York, 1993.

G. J. Nathan, S. R. Turns, and R. V. Bandaru. "The influence of fuel jet pressessing on the global properties and emissions of unconfined turbulent flames," *Combust. Sci. & Tech.*, 112, 211–230, 1996.

P. R. Owen. "Saltation of uniform grains in air," *J. Fluid Mech.*, 164, 20(2) 225–242, 1964.

F. P. Ricou and D. B. Spalding. "Measurements of entrainment by axisymetrical turbulent jets," *J. Fluid Mech.*, 11, 21–32, 1961.

H. Schlichting. *Boundary-Layer Theory*. McGraw-Hill, New York, 1979.

G. M. Schneider. *Flow Structure and Turbulence Characteristics in a Precessing Jet*. Ph.D. Thesis, University of Adelaide, 1996.

R. R. Sood, D. M. Stokes, and R. Clark. "Static design of coke calcining kilns," Internal Report, Alcan International, Arvida, Canada, 1972.

E. N. Tackie, A. P. Watkinson, and J. K. Brimacombe. "Mathematical modeling of the elutriation of fine materials from rotary kilns," *Can. J. Chem. Eng.*, 68, 51–60, 1990.

M. W. Thring and M. P. Newby. "Combustion length of enclosed turbulent jet flames," *4th Int'l Symposium on Combustion*, Baltimore, pp. 789–796, 1953.

B. G. van der Hegge Zijnen. "Measurement of the distribution of heat and matter in a plane turbulent jet of air," *Appl. Sci. Res.*, A.7, 256–313, 1958.

R. Videgar. (1997). "Gyro-therm technology solves burner problems," *World Cement* (November), 1997.

L. Zhou. *Theory and Numerical Modeling of Turbulent Gas-Particle Flows and Combustion*. CRC Press, Boca Raton, FL, 1993.